University of Baghdad
College of Engineering
JOURNAL OF ENGINEERING

Journal of Engineering
journal homepage: www.jcoeng.edu.iq
Volume 31 Number 10 October 2025

Numerical Study of Various Steel Plate Configurations for Rejoining an Asymmetrical Steel Section - Composite Concrete Beams

Wisam Hazim Khaleel *, **Ahmad Jabbar Hussain Alshimmeri**

Department of Civil Engineering, College of Engineering, University of Baghdad, Baghdad, Iraq

ABSTRACT

This study numerically investigates the effect of different welding steel plate shapes on the behavior of expanded open web asymmetrical steel composite beams. Increased web depth of asymmetrical steel beams in composite concrete results in increased stiffness and strength. Expanding the web's depth enhances the composite concrete steel beam's strength and performance in specific design scenarios, such as expanded, cellular, or castellated steel composite concrete beams. A horizontal cut in the web in each asymmetrical section can create an expanded web of asymmetrical steel profiles. Two asymmetrical tees can then be assembled, and a plate known as a spacer plate with a constant area and different shapes can be added between the two halves of the asymmetrical tee sections. The Finite Element (FE) numerical model developed by ABAQUS software was employed to develop and evaluate new numerical models by considering a variety of increment plate configurations, which resulted in the production of a greater number of models at a lower cost and more efficiently. The results indicate that curved plates increased the ultimate load capacity, while other shapes led to decreased stiffness. Therefore, the ultimate load capacity of the curved plate increased by approximately 2.3% compared to the reference model due to a reduced stress distribution.

Keywords: Concrete composite beam, Concrete damage plasticity, Expanded web, Finite element modeling, Web buckling

1. INTRODUCTION

Since the early 1920s, steel-concrete composite constructions have been utilized in bridges and buildings **(Ollgaard et al., 1971)**. The Expanded Steel Beam (ESB) allows service pipes, cables, and ventilation ducts to pass through web openings, lowering the floor height of buildings when compared to a solid web beam. Additionally, it is a practical method of lowering steel use. The web plate's continuity in an ESB was broken by the web openings. A Solid Web Steel Beam (SWSB) and an ESB have common strength and stability failure modes,

*Corresponding author
Peer review under the responsibility of University of Baghdad.
https://doi.org/10.31026/j.eng.2025.10.05

Article received: 05/04/2025
Article revised: 16/06/2025
Article accepted: 22/06/2025
Article published: 01/10/2025

but an ESB would also experience three additional failure modes: shear rupture of the web-post's weld, Vierendeel mechanism failure at the perforated section, and web-post buckling failure **(Nethercot et al., 1984; Redwood et al., 1998; Abidin et al., 2013)**. Research on the composite concrete-expanded open web steel beam's lower flange's distortional buckling was also crucial **(Al-Zuhairi et al., 2017; Oukaili et al., 2017)**. Many studies on web-post buckling behavior in castellated steel beams with conventional hexagonal or circular web apertures have been published. Different factors that could affect the bulking behavior of web posts have been studied **(Tsavdaridis et al., 2012; Al-Tameemi et al., 2023)**, including the opening distance, the web height–to-thickness ratio, and the opening size and shape. Many novel techniques have been used to increase steel members' stiffness without significantly increasing their weight. Consequently, steel beams featuring web openings, commonly referred to as castellated or cellular beams, have been extensively utilized. Primary advantage of utilizing apertures in beams during construction is the integration of services, including electrical cables, ventilation ducts, and hydraulic pipes, inside the specified depth of the beams **(Ahmed et al., 2024)**.

Furthermore, the reinforced concrete beams may have holes in regions where the stresses are minimal or have a negligible effect, so further enhancing structural efficiency **(Abdul-Razzaq et al., 2023; Dawood et al., 2024)**. **(Dinehart et al., 2004)** investigated the stress distribution at cellular beam apertures under different combinations of loads. Clarifying the critical status of a typical circular cell under load conditions was the main goal of this effort. **(Basher et al., 2009)** investigated how the ultimate load capacity of composite plate girders with horizontal curvature was affected by square and circular web apertures. The beams' ultimate strength functions and behavior were investigated using FE analysis with the LUSAS program when the net opening was of varying proportions. Recall the impact of grid opening and the general interaction between steel beam and concrete slabs. Additionally, that provides an estimation technique for determining the final power capacity of the total plate beams with horizontal curvature. The function's accuracy is evaluated in contrast to the necessary power, as evidenced by the values accomplished through the FEM. According to the study, web cut-outs significantly reduce shear capability in high shear zones. The suggested approximation approach can accurately predict the ultimate shear strength of composite plate girders with horizontally curved with web perforations.

(Hagen et al., 2009) conducted a design model for steel girders with web openings containing single and multiple openings with different shapes, stiffeners, and double plates was developed by means of numerical simulations. Results on distribution of transverse web deformation, ultimate shear capacity, and von Mises stresses were shown; the model was intended to preserve pure shear at the opening center. The model considers opening position, shear buckling, and reduction in web shear area, vertical stiffness, and opening reinforcements. The simulations ran with the FE program ABAQUS **(Hagen et al., 2009)**. **(Radic et al., 2008)** conducted a numerical analysis of castellated beams, comparing two distinct methodologies for calculating the elastic critical moment for lateral-torsional buckling against Eurocode 3 procedures and finite element results **(Fang et al., 2022)**. **(Abbas and Alshimmeri, 2024)** tested the flexural performance of a composite concrete-reinforced asymmetrical castellated steel beam made by attaching two castellated hot-rolled steel channels back-to-back: a built-up I-shaped configuration with a 52.4% beam depth increase. Four examples were tested: a reference specimen without reinforcement, a specimen fortified with Reactive Powder Concrete (RPC) in the steel web area, and a third with RPC reinforced by lacing rebar. By applying two-point static stresses to the composite

beams' concrete deck slab, all specimens were tested under simply supported conditions. The second and third specimens had higher stiffness, ductility, and energy absorption than the first, increasing their ultimate load capacity by 24.01% and 48.34%, respectively. Fourth specimen (reinforcement without welding in web posts) had worse stiffness and ductility than first specimen (control) due to 11.02% lower ultimate load capacity. **(Naji and Al-Shamaa, 2025)** analyzed the structural efficacy of castellated steel beams with expanded webs, emphasizing the impact of design variables, such as aperture quantity and cutting angle, on load-bearing capacity, deflection, and stiffness. Castellated beams are engineered to improve the strength-to-weight ratio of traditional I-beams by altering the web into hexagonal, rectangular, or circular openings. This design enhances beam load capacity and minimizes weight while maintaining or augmenting rigidity, rendering it suitable for long-span structures. This study entailed the examination of seven beam specimens subjected to a single-point load, including six castellated beams. The primary findings demonstrate that reducing the number of holes significantly improves load capacity and diminishes deflection. The castellated beams surpassed the control sample by up to 68.9% in load-bearing capacity at Service Limit Deflection (SLD). The research examined the influence of cutting angles (58°, 52°, and 45°) on beam performance, concluding that a 52° angle provided the ideal balance between strength and stiffness.

This study investigates the different opening shapes of composite concrete beams – asymmetrical steel sections with expansion web by adding increments steel plates (spacer plate) and investigates different steel plate shapes (spacer plate) with constant dimensions steel plates under point load and above supports at 100 mm and 200 mm, respectively. The increments of steel plates (spacer plate) and opening shapes were kept constant in their area, with variable shapes.

2. EXPERIMENTAL PROGRAM

An experimental model of a composite concrete beam with an enlarged open web asymmetrical steel section was cast and tested to validate the FE model and compare the results with the experimental data. The specimen's clear span length was 250 cm, and its overall length was 270 cm. It was tested under two-point load. The experimental model possesses identical dimensions and reinforcement as the numerical model.

2.1 Asymmetrical Steel Section

This study utilized rolled standard steel (IPE180) and (IPE200) to fabricate steel beams with an expanded web as shown in **Fig. 1**. The characteristics are presented in **Tables 1 and 2**

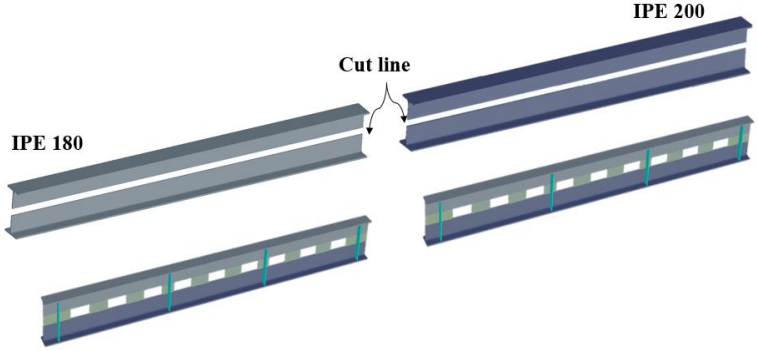

Figure 1. Fabrication process of steel section with expansion web

2.2 Plates

Plates were utilized as stiffeners to execute the strengthening process and reconnect the asymmetrical steel section by welding a spacer plate between them. The expansion ratio was 50% of the parent steel section, and the dimensions of the steel plates, which were reconnected between different halves of the asymmetrical steel section, according to the castellated steel limitation. The steel plates were chosen to achieve the ratio of length plate steel to web thickness between ratios (10-30). Therefore, the steel plate (spacer) length was 140 mm for positions between load and supports, and for positions under point load, 100 mm, and above supports were chosen at 200 mm. Their attributes are detailed in **Table 3**.

2.3 Fabrication of Expanded Web Steel Section

A control numerical cutting (CNC) plasma- machine for two IPE was used to linearly cut the web section along its centerline in a horizontal pattern in order to create the steel beam with an expanded web specimen for the experimental work. The two halves were then divided, as **Fig. 1** illustrates. To create steel beams with expanded web specimens that include openings, an increment plate was inserted between the two different types of horizontally cut web halves, and all of them were welded together with 3 mm-thick welding (ASTM A36/A36M-14).

2.4 Concrete Desk Slab

In a composite system, an effective connection between the two parts is crucial. As a result, shear connections made of a 40 x 30 x 3 mm steel channel section, totaling 50 mm in length, were positioned 150 mm c/c apart at the top surface of the steel I-beam, perpendicular to each other. The concrete deck slab measured 450 mm in width and was reinforced in both directions with 8 mm-diameter deformed steel bars positioned 100 mm apart with a compressive strength of 32 MPa.

2.5 Test Setup

The specimen was tested at the University of Diyala's Civil Engineering Department's structure lab. Static load was applied during the testing process using a 600 kN load cell and a hydraulic jack universal. Until the beams failed, the load rate was 0.25 kN/s. Several measures, such as load and the deflection at the center of the beam, were taken during the testing. As shown in **Fig. 2**, a two-concentrated load was applied to the beam.

Table 1. Asymmetrical steel sections characteristic.

Section	G, (Kg/m)	h, (mm)	B, (mm)	, t_w (mm)	, t_f (mm)	r, (mm)	A, $(mm)^2$	$I_x \times 10^4$ $(mm)^4$	$S_x \times 10^3$ $(mm)^3$	$Z_x \times 10^3$ $(mm)^3$
IPE180	18.8	180	91	5.3	8	9	2390	1317	146.3	166
IPE200	22.4	200	100	5.6	8.5	12	2850	1943	194.3	221

Table 2. Properties of steel sections.

Part	Yield stress (MPa)	Ultimate stress (MPa)	Modulus of elasticity (MPa)	Elongation %
IPE180	360	462	200000	23
IPE200	376	480	200000	26

Table 3. Properties of steel plate and rebar.

Part	Thickness (mm)	Yield stress (MPa)	Ultimate stress (MPa)	Elongation %
Plate (stiffeners, web post)	5.8	310	380	24
Rebar (concrete slab)	8 diameter	450	623	21

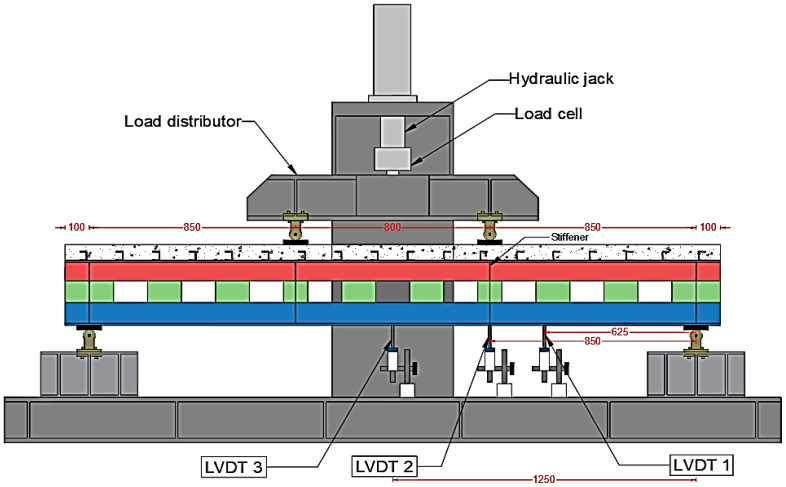

Figure 2. Experimental test setup profile

2.6 Designation of Specimens

Designation of all models were named based on the shape of steel plate which to re-joint (spacer plate) asymmetrical steel section with kept constant shape under point load and supports, as shown in **Figs. 3 to 10**.

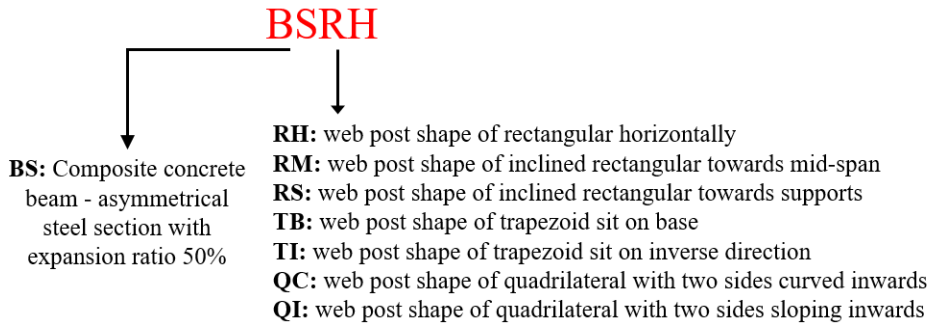

Figure 3. Designation of all models

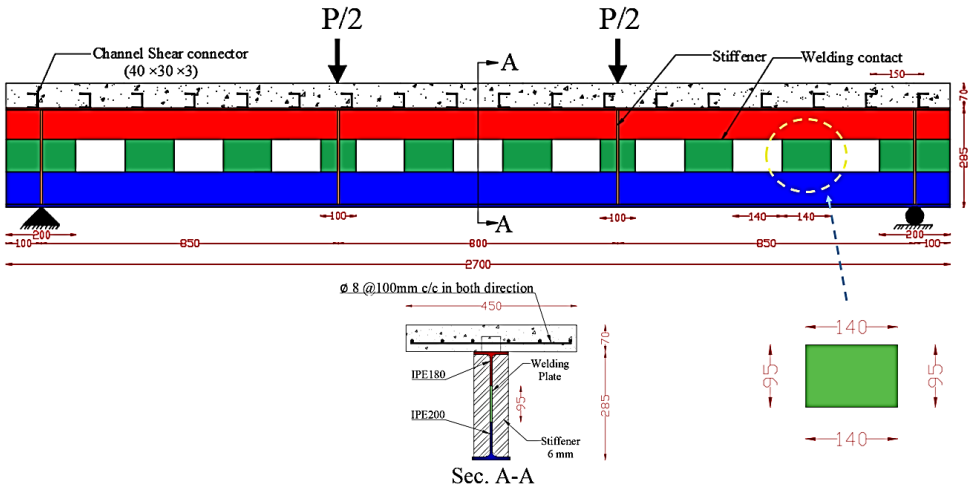

Figure 4. Positions load and support with dimensions of the model BSRH

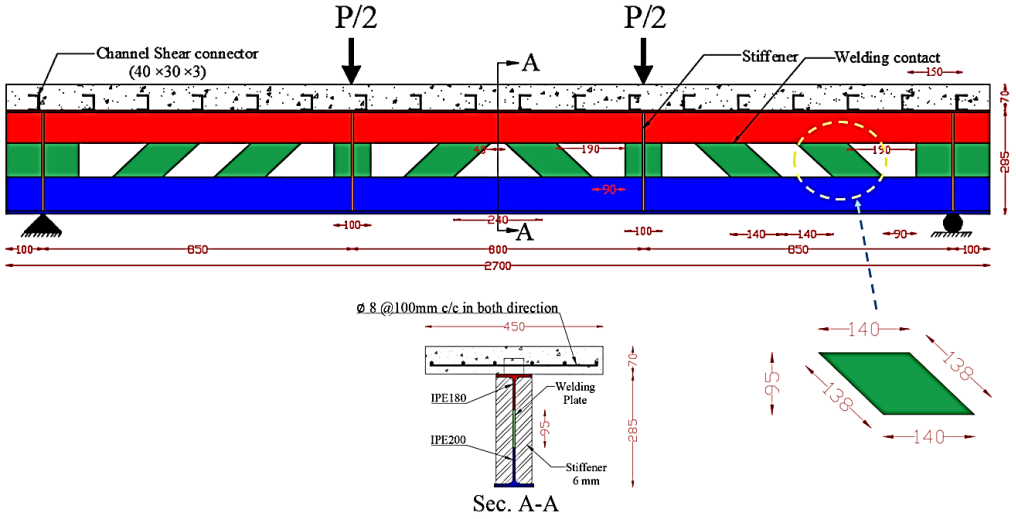

Figure 5. Positions load and support with dimensions of the model BSRM

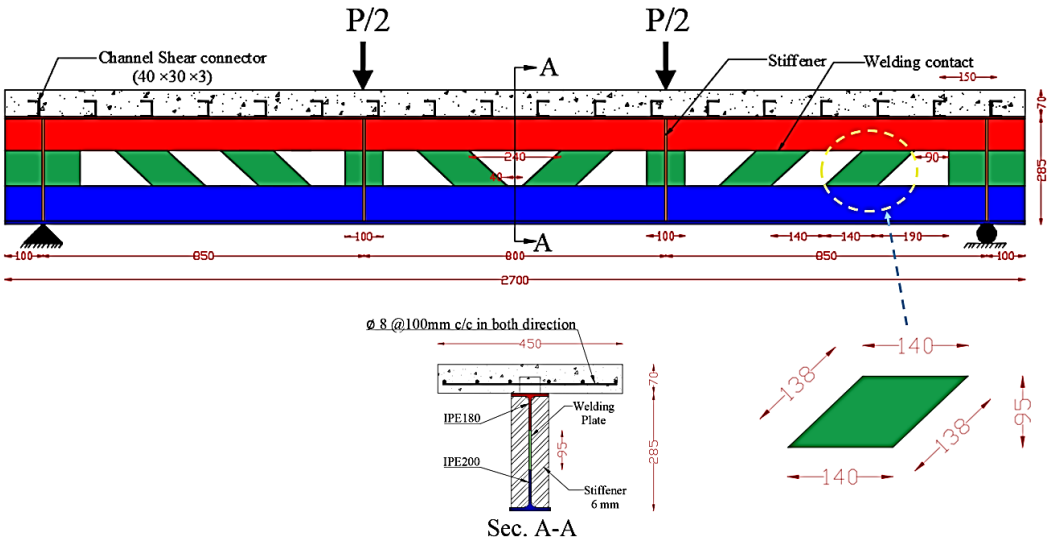

Figure 6. Positions load and support with dimensions of the model BSRS

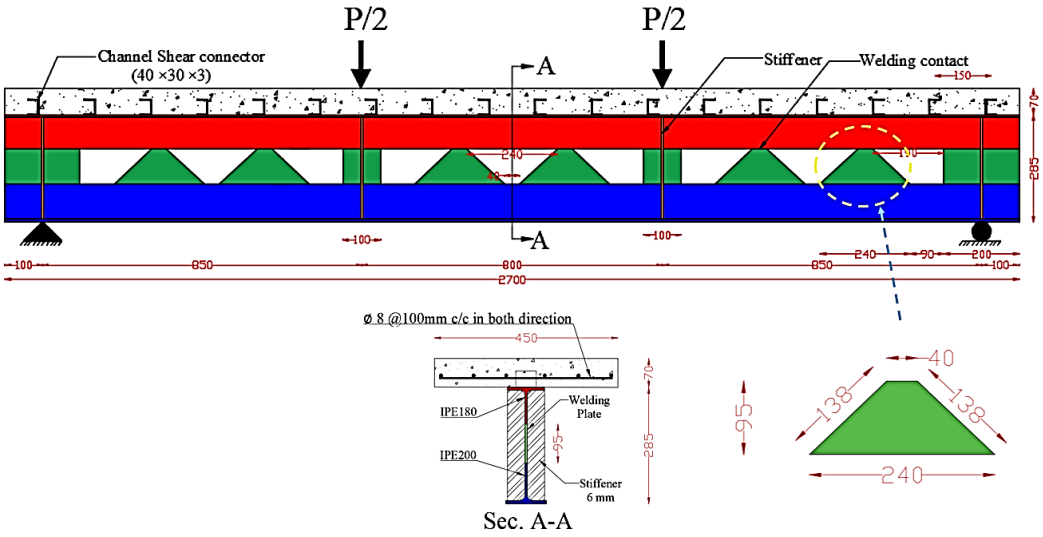

Figure 7. Positions load and support with dimensions of the model BSTB

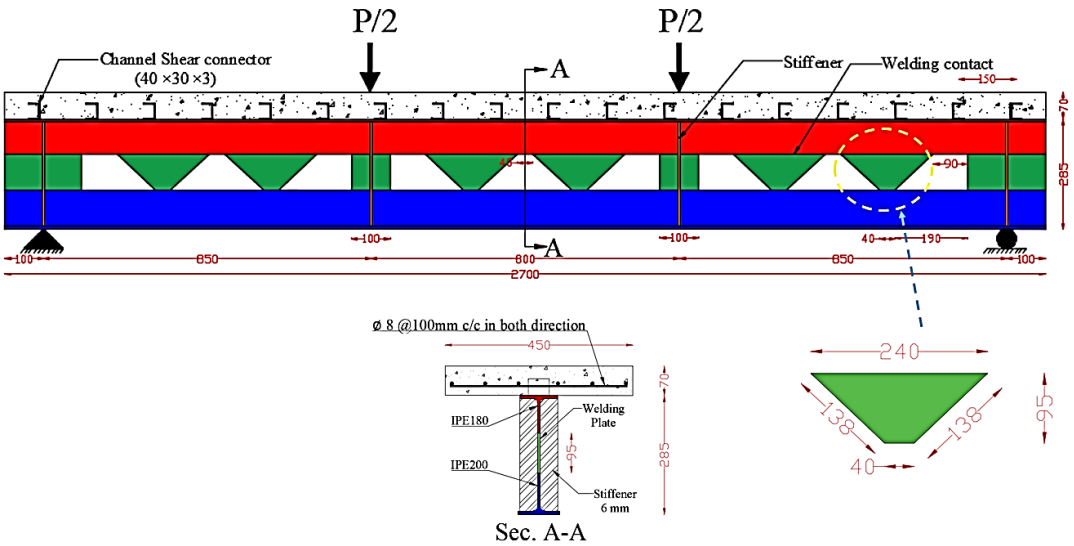

Figure 8. Positions load and support with dimensions of the model BSTI

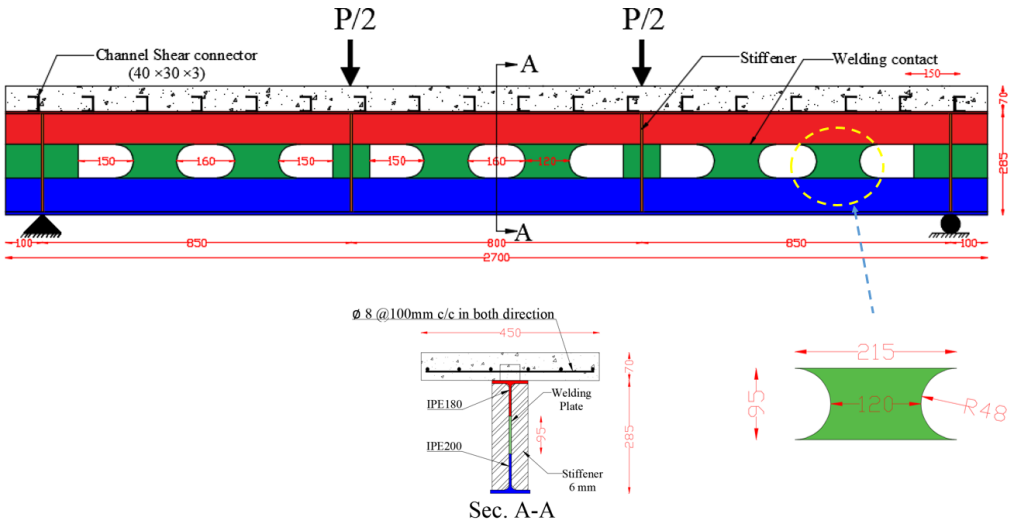

Figure 9. Positions load and support with dimensions of the model BSQC

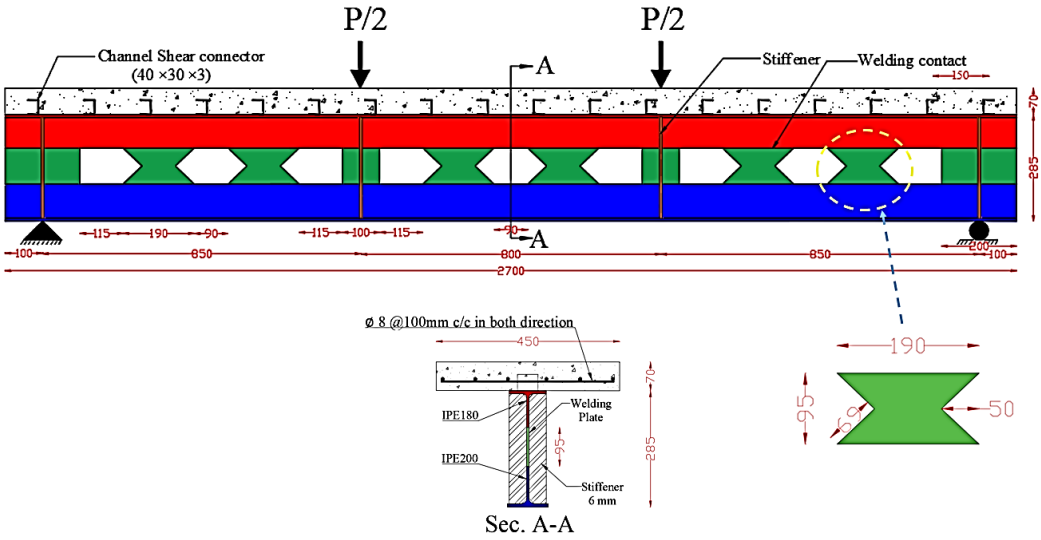

Figure 10. Positions load and support with dimensions of the model BSQI

3. FINITE ELEMENT

3.1 Geometrical Modeling

The initial step in FE is to describe the geometric components of the specimen that is being tested. **Fig. 11** displays the finite element model of the tested beam, including all of its components, subjected to a static load.

3.2 Material Modeling

Concrete undergoes strain-softening in compression and tension and stiffness degradation under all stress conditions, with the exception of hydrostatic pressure **(Lubinar et al., 1989; Al-Hilali and Izzet, 2023)**. The Concrete Damage Plasticity Model (CDPM) was developed in the Abaqus program to allow for the former behavior of other quasi-brittle materials and other concrete. **Fig. 12** shows that for compression and tension, the damage parameters d_c and d_t reflect the deterioration process in the elastic stiffness. The mathematical expression of the damage parameters is challenging.

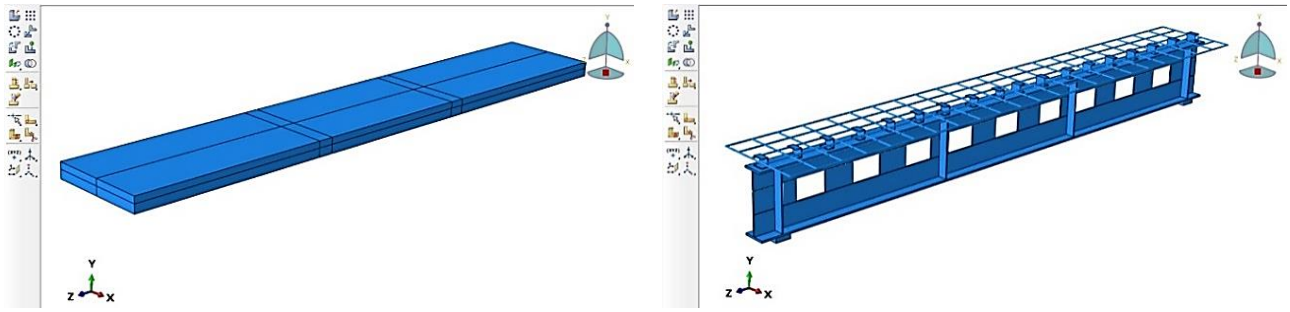

(a) **(b)**

Figure 11. Finite element idealization of composite concrete-asymmetrical steel section with expansion web (a) concrete desk slab (b) steel sections and rebar

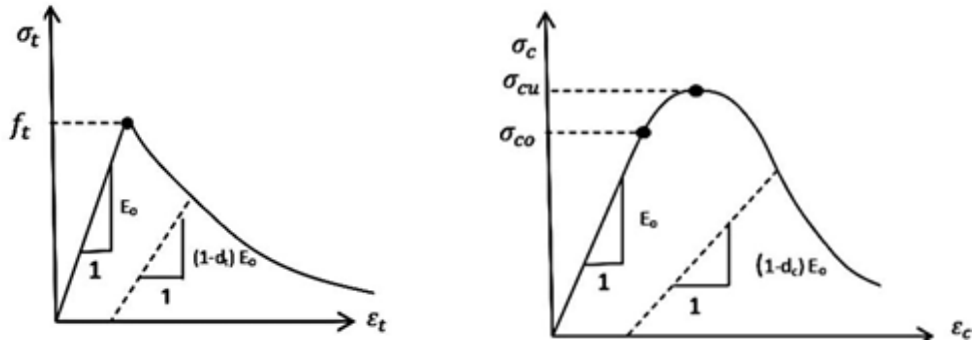

(a) (b)

Figure 12. Concrete behaviours: (a) under uniaxial tension, (b) under uniaxial compression. **(ABAQUS, 2017)**

However, the parameters d_c and d_t were given a simpler expression by **(Hafezolghorani et al., 2017)**. The suggested model states that no damage to stiffness occurs before to the apex of the stress-strain curve, and the parameters are assessed using Eq. (1).

$$d_{c,t} = 1 - \frac{\sigma_{c,t}}{\sigma_{u\ c,t}} \tag{1}$$

where; σ is concrete stress (N/mm^2), σ_u is the stress at ultimate (N/mm^2), and the letters t and c describe tension and compression, respectively.
In tension, $\sigma_u = f_t$. The present work evaluates and specifies the damage parameters dt (tensile deformation) and d_c (compression deformation) using this formula.
Five plasticity parameters are required by the CDPM model in order to ascertain the plasticity characteristics of concrete, mainly:

- The dilation angle (ψ): denotes the internal friction angle of the material; so, it shows that the plastic volume of concrete has risen more than the critical stress value. **(ABAQUS, 2017).** Simulations usually advise ψ = 20° to 40°, which affects the elasticity of the material. The general model was therefore much affected by the dilation angle. The system's adaptability increased with the rising dilation angle. **(Haftezolghorani et al., 2017)** Still, more recent research has successfully applied higher values of ψ. Selected for usage with reinforced concrete a value of =56^o **(Demir et al., 2016)**. After several studies, 35^o turned out to be the perfect value for our project.
- Eccentricity is a quantity known as flow potential eccentricity, which is defined as the flow potential G tends to a straight line when the eccentricity tends to zero (0.1 is the default value of eccentricity) **(Hafezolghorani et al., 2017)**
- fb0/fc0 is the ratio of initial equibiaxial compressive strength to initial uni-axial compressive strength (the default value is used in analysis 1.16).
- Kc: is the ratio of the second stress invariant on the tensile meridian, (TM), to that on the compressive meridian, $q(CM)$. This study adopted a default value of two thirds.
- The viscosity parameter, which indicates the viscoplastic system's relaxation time and typically aids in accelerating the beam model's rate of convergence in the softening zone, is taken to be zero as the beam model did not result in significant convergence issues. Thus, in the present analysis, no viscoplastic regularization is done, and value of μ =0.008 was adopted.

3.2.1 Concrete's Compressive Behavior

A concrete's stress-strain, as seen in **Fig. 13** and proposed in Eq. (2), can be used to determine uniaxial compressive behavior using an existing constitutive model that was proposed by **(Hognestad, 1951)**. This model has been used in this simulation.

$$\sigma_c = f_c' \left[2\left(\frac{\varepsilon_c}{\varepsilon_0}\right) - (\frac{\varepsilon_c}{\varepsilon_0})^2\right], \varepsilon_0 = \frac{2f_c'}{E_c} \quad (2)$$

where; σ_c nominal concrete compressive stress (N/mm²). E_c : Modulus of elasticity of concrete (N/mm²). f_c': Concrete's compressive strength (the unconfined cylinder specimen) (N/mm²). ε_0 : Strain at peak stress (the strain at the curve's peak point). ε_c : Nominal compressive strain in concrete. Assumed from start to finish was the equation describing concrete's non-linear behaviour.

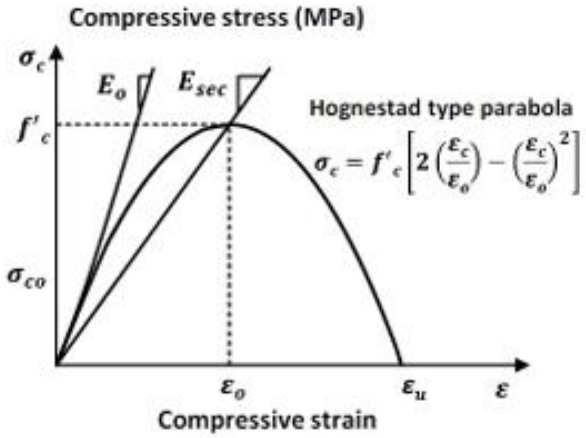

Figure 13. Hognestad Parabola **(Hognestad, 1951)**

According to this investigation, the linear component is considered to be up to a stress of 0.40. Concrete's modulus of elasticity is equivalent to its secant modulus; it is the inclination of the line segment between the beginning point and the point on the curve where the stress is $0.40f_c'$. Eq. (3) **(Hejazi et al., 2017)** helped one to ascertain the inelastic strain. A strain concrete crushing of 0.0035 was employed in accordance with the between of (0.003) to (0.004) specified in the ACI code **(ACI M318, 2019)**.

$$\varepsilon_c^{in} = \varepsilon_c - \frac{\sigma_c}{E_0} \quad (3)$$

As illustrated in **Fig. 13**, damage resulting from greater plastic strains in semi-brittle materials is represented by a decrease in the curve's tangent with respect to the initial diamond (modulus of elasticity, E_0). The damage parameter (d_c) was zero at the apex of the curve (i.e., ultimate compressive stress f_c'); it then progressively dropped to 0.8, indicating 20% strength remaining in huge strain **(Hejazi et al., 2017)**.

3.2.2 Tensile Behavior of Concrete

Though events like aggregate interlocking in cracks and concrete-steel adhesion between fractures are taken into account, concrete under tension is not considered as brittle-elastic.

Hence, the stress-strain reduction in the tension zone occurs gradually instead of all at once.
One-tenth that of the comparable compressionf_c' is (ε_{cu}), The following Eq. (4) is used to evaluate ε_{cu}:

$$\varepsilon_{cu} = 0.012 - 0.001 f_c' \quad (4)$$

The strain at failure determined from the material characteristics is (3.86/22960 = 1.68 × 10^{-4}); it is 9.16 times ε_{cr} ,. **(Alkloub et al., 2019)** applying a 0.00154 ultimate cracking strain. Eq. (5) is used to evaluate the cracking strain ε_{cr} at every given position.

$$\varepsilon_{cr} = \varepsilon_t - \frac{\sigma_t}{E_0} \quad (5)$$

3.2.3 Steel Sections and Reinforcement Modeling Properties

The asymmetrical steel sections, reinforcements, and channel have been numerically modelled as elastic-perfectly plastic, as illustrates in **Fig. 14 (ABAQUS User Manual, 2017)**. As illustrated in **Fig. 14**, this is consistent with the von Mises failure, which considers the material's elastic behavior until the yield stresses are reached, at which point it becomes completely plastic. The linear isotropic component is determined by the modulus of elasticity and Poisson's ratio of the reinforcement and asymmetrical steel sections material, which have been determined to be 205×10^3 N/mm^2 and 0.3, respectively. The bilinear isotropic component is characterized by yield stress, as demonstrated in the experimental test. Additionally, linear isotropic materials are used to approximate the steel bearing and support plates. The same numbers are used by the reinforcement material to mimic linear isotropy for the Poisson's ratio of 0.3 and the modulus of elasticity of 200×10^3 N/mm^2.

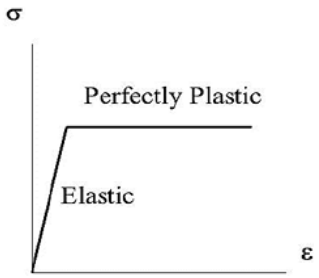

Figure 14. Stress – strain curve of an asymmetrical steel section and reinforcement

3.2.4 Boundary Conditions and Load Application

The external load application and boundary conditions used in the simulation were the same as those used in experimental tests. One of the support components was modeled as a roller, and the other as a hinge. To achieve simulated hinge support, (Uy=Ux= Uz=0) was utilized to guarantee the restricting of one of the supports and serve as the roller support (Uy=Uz=0). A displacement-controlled load is applied to the upper surface of steel loading plates under static loading.

3.3 Meshing and Interaction of the Model

The mesh module contains the tools needed to create meshes on the generated components and assemblies. There are numerous ABAQUS software versions that can be used, and it is crucial to select the one that best fits the problem. All of the model components, with the

exception of steel reinforcements, are modeled using typical two-dimensional features. The asymmetrical steel profiles and the concrete slab are modeled using three-dimensional stress elements. This section examined several numerical model parameters that could affect the prediction of overall behavior and ultimate load on the reference specimen. Five gradually improved meshes were tested: 50 mm, 35 mm, 25 mm, 15 mm, and 10 mm. The optimal mesh size (25 mm) was first determined through mesh sensitivity studies. The solid components are not chosen because they are difficult to comprehend from a mathematical standpoint. Due to the fact that reinforcement bars do not possess a high flexural stiffness and that their attachment to concrete must be properly bonded, truss components have been utilized and modeled as embedded elements. In order to create the FE models for the asymmetrical steel section, the concrete slab, and the support plates, linear brick hexahedral C3D8R elements were selected. These elements are continuum elements (C) with 3D eight nodes (8) and reduced integration (R). T3D2 elements, on the other hand, are elements (T) with two 2D nodes (2) that were chosen for the steel reinforcing bar finite element models. T3D2 and C3D8R elements are displayed in **Fig. 15** and **Table 4**. The contact between the steel segment and the concrete slab was established using the "contact pair" algorithm. "When selecting the master and slave surface, it is important to consider the stiffness of the structure rather than solely the material," states the ABAQUS analysis user's manual. Because of this, the top of the steel section was regarded as a slave surface and the bottom of the concrete slab as a master surface. Using a finite sliding method, surface-to-surface contact was employed. The behavior is normal and tangential to the surfaces described the interaction between these two contacting surfaces, which are the top of the steel section and the bottom of the concrete slab. The "hard" contact pressure-overclosure relationship was the default typical behavior that was presumed. Through this type of specific behavior, the smallest amount of slave surface in the main surface was secured. According to the penalty friction, the friction coefficient between the steel section and concrete slabs was determined to be 0.6. For tangential and normal behavior, respectively, contact between steel section and concrete slabs was described as "hard" contact interactions and friction - contact interactions **(Li et al., 2024)**.

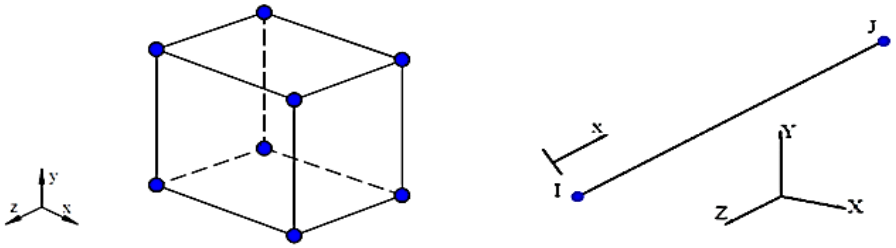

(a) Solid element (b) Truss element

Figure 15. Type element for modelling

Table 4. Details of the element in FE.

Component	Family	Characteristics of element
Asymmetrical steel profile, concrete, bearing plates, and steel channel	3D Stress	C3D8R: A three-dimensional, eight-node, linear, brick with a continuum, reduced integration, and hourglass control.
Reinforcement bars	Truss	T3D2: A tie, three-dimensional, 2 - node linear truss

4. VALIDATION OF MODEL

A comparison is made between the numerical analysis and experimental results in terms of failure load and load deflection curves. Finite element analysis yielded theoretical findings that were in good agreement with experimental values, with differences of 1.012 and 0.95 for ultimate loading and deflection, respectively. The FE analysis and experimental findings are summarized in **Table 5**. The failure mode of experimental BSRH was welding web-post failure with a longitudinal crack in a concrete slab that happened at the final loading stage due to increasing flexural strength, **Fig. 16**. The experimental data was contrasted with the FEM results, **Fig. 17**. In the majority of instances, the load-deflection that the FEM predicted matched the actual outcomes. Its response, however, was stiffer than those, **Fig. 18.**

Table 5. Experimental and FE results

Specimen	Results related to	Peak load P (kN)	FE/Exp.	, at ultimate Δ load (mm)	FE/Exp.	Status
BSRH	FE	308.4	1.012	18.54	0.95	Reference
	Exp.	304.7		19.34		

Figure 16. Mode failure of BSRH experimentally

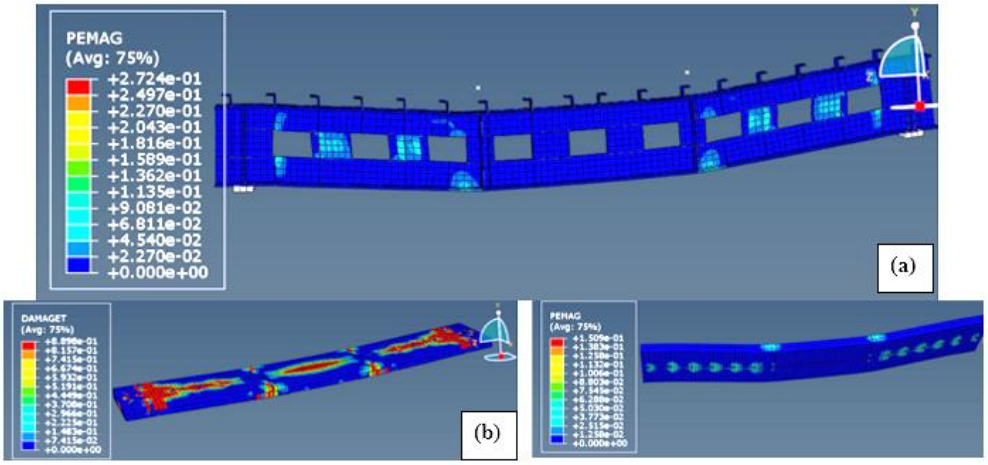

Figure 17. Mode failure of FE for BSRH specimen (a) Asymmetrical steel section (b) Concrete deck slab

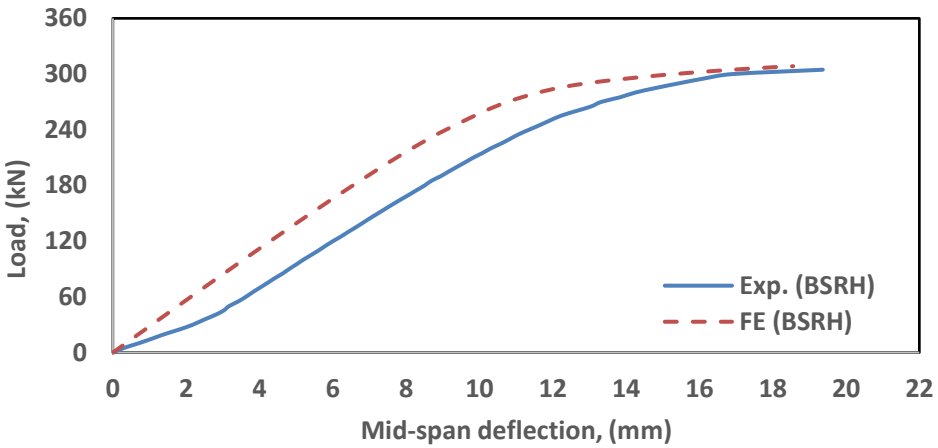

Figure 18. Load-deflection curve of Exp. and FE specimens

5. RESULTS AND DISCUSSION

5.1 Ultimate Load

The ultimate load for each numerical analysis model is displayed in **Fig. 18**. The ultimate load in models BSQC is roughly 2.30% larger than in Ref. model BSRH because web-post shape curves are used to prevent stress concentration, **Table 5**. The ultimate decreased by about (3.14%, 4.27%, 20.45%, 20.29%, and 1.98%), respectively, for BSRM, BSRS, BSTB, BSTI, and BSQI in comparison with the reference BSRH. This decrease led to web-post shape, especially specimens BSTB and BSTI, necking in its dimensions and concentration distribution of stresses, as illustrated in **Fig. 19** and **Table 6**.

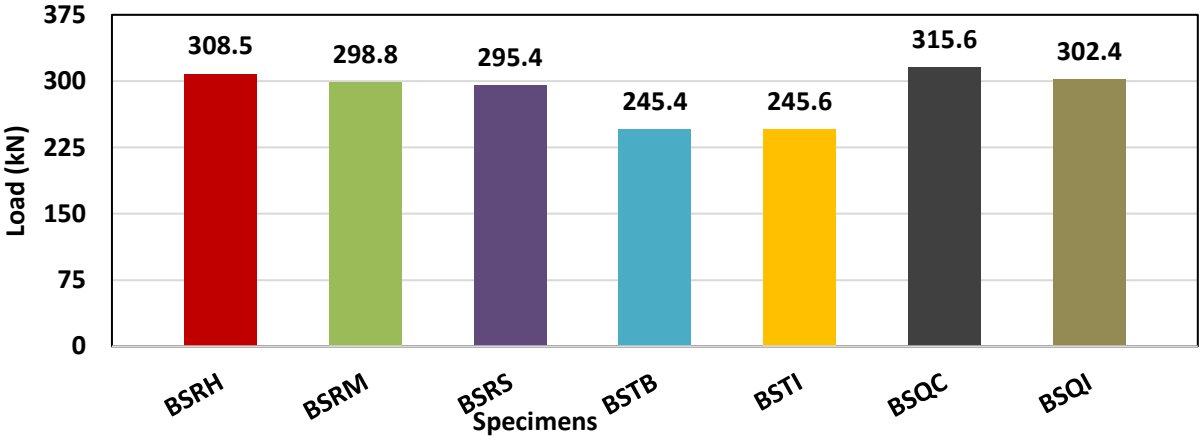

Figure 19. Ultimate load for specimens

Table 6. Comparison of the load of all specimens

Model ID	Ultimate load (kN)	Differences in Peak load %
BSRH (Ref.)	308.5	---
BSRM	298.8	- 3.14
BSRS	295.3	- 4.27
BSTB	245.4	- 20.45
BSTI	245.9	- 20.29
BSQC	315.6	+ 2.30
BSQI	302.4	- 1.98

5.2 Failure Mode and Deflection

The ultimate deflectionΔ_u, فhe deflection at peak load was increased by (7.04%, 13.56%, 18.02%, 24.37%, 5.32, and 18.74%), respectively for specimens BSRM, BSRS, BSTB, BSTI, BSQC, and BSQI in comparison with the reference specimen BSRH, as shown in **Table 7** and **Fig. 20**. The deflection findings for analytical models from the initial load to the final load are shown in **Figs. 21 to 27**. **Table 7** describes the deflection failure scenarios.

Table 7. Summary of deflection and failure mode for all specimens

Model ID	Defl. at peak load Δ_u (mm)	Difference in Δ_u %	Failure mode
BSRH (Ref.)	17.48	---	Flexural mechanism, yielding at web-post, and yield at bottom tee
BSRM	18.71	+ 7.04	Flexural mechanism, yielding at web-post, yielding at bottom tee, and shear
BSRS	19.85	+ 13.56	Flexural mechanism, yielding at web-post, yielding at bottom tee, and shear
BSTB	20.63	+ 18.02	Flexural mechanism, local buckling at web-post, and yield at bottom tee
BSTI	21.74	+ 24.37	Flexural mechanism, local buckling at web-post, and yield at bottom tee
BSQC	18.41	+ 5.32	Flexural mechanism, and yield at bottom tee
BSQI	18.74	+ 7.21	Flexural mechanism, and yield at bottom tee

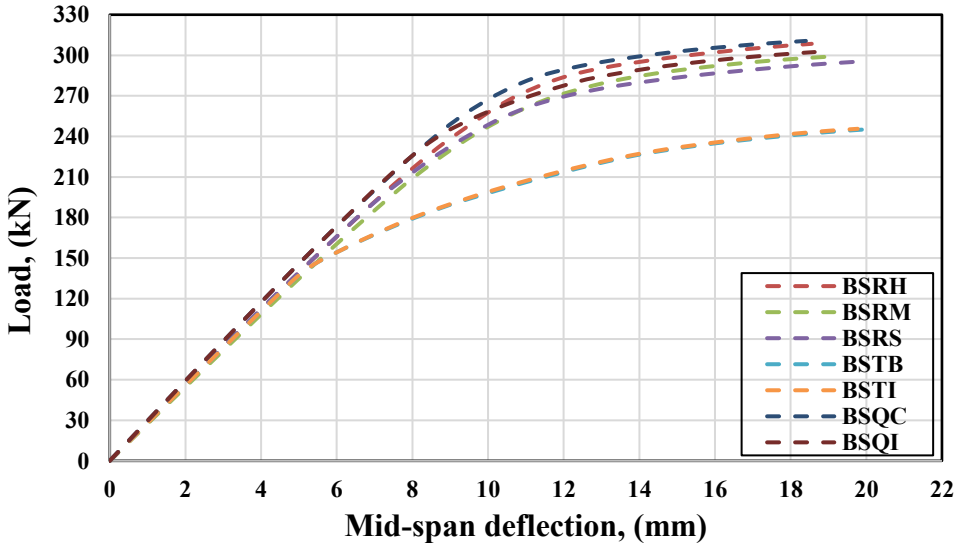

Figure 20. Load-deflection curve of all FE specimens

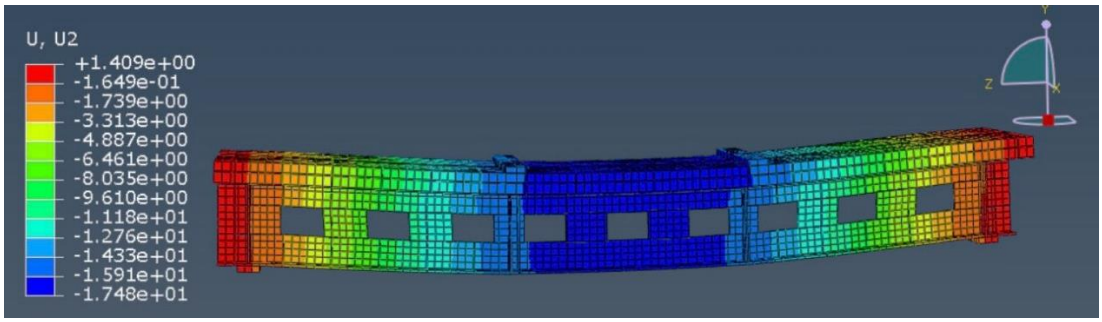

Figure 21. The deflection values along the model BSRH at peak load

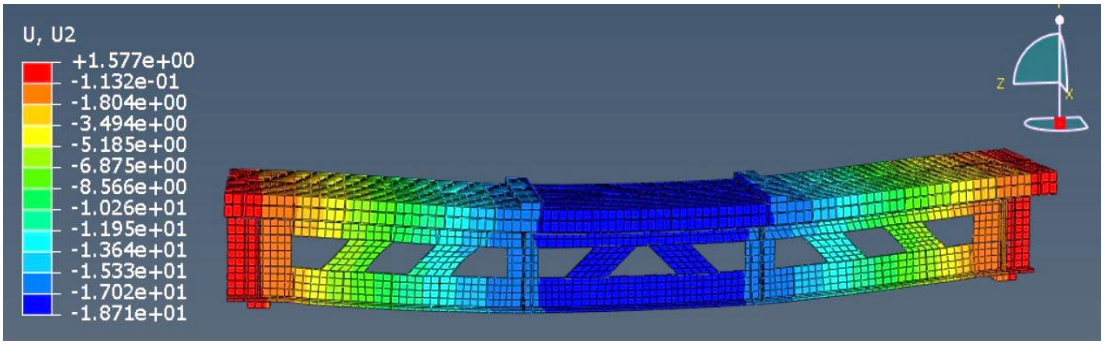

Figure 22. The deflection values along the model BSRM at peak load

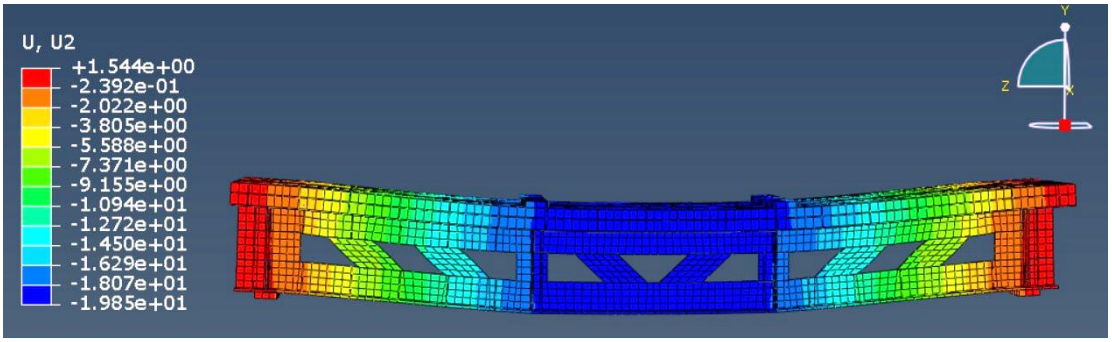

Figure 23. The deflection values along the model BSRS at peak load

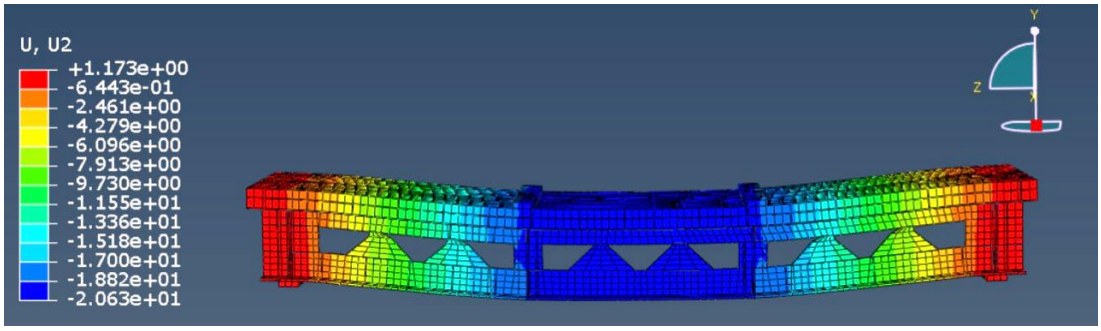

Figure 24. The deflection values along the model BSTB at peak load

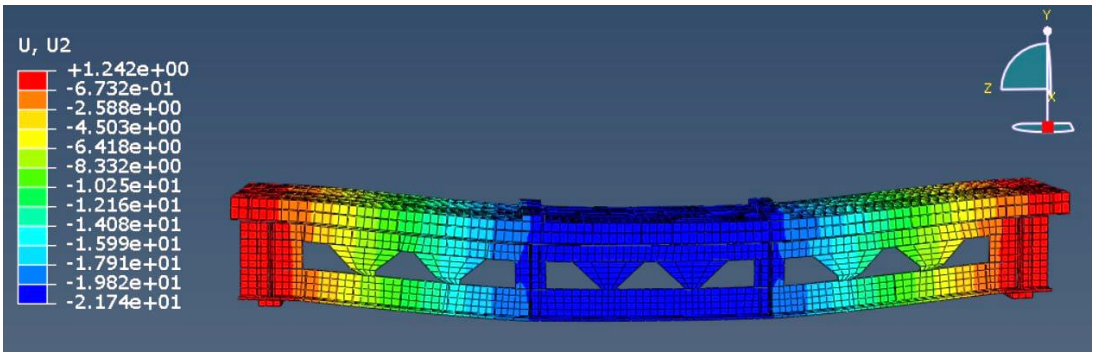

Figure 25. The deflection values along the model BSTI at peak load

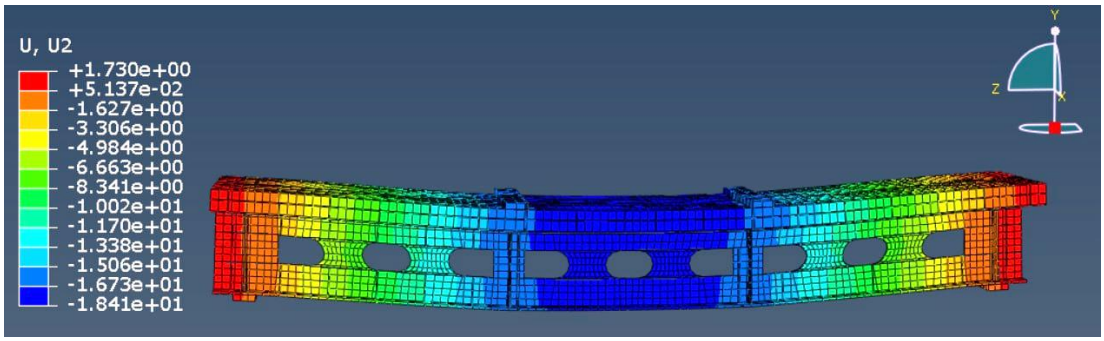

Figure 26. The deflection values along the model BSQC at peak load

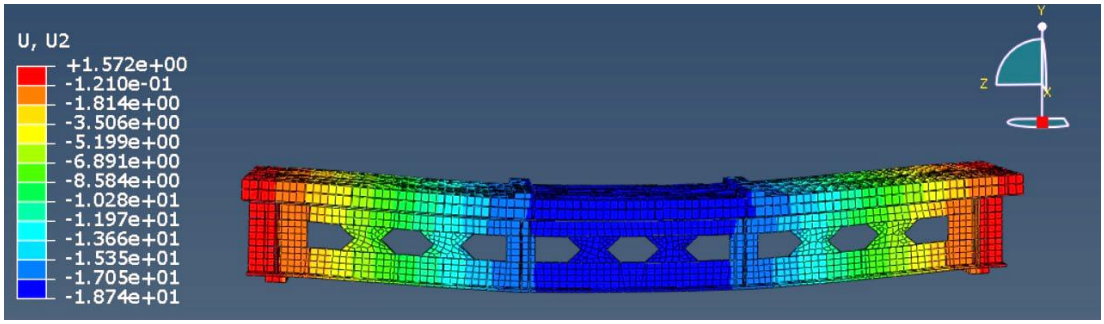

Figure 27. The deflection values along the model BSQI at peak load

5.3 Stiffness

The load required as a result of unit deflection is called stiffness **(Abbas and Alshimmeri, 2024)**. Peak load and deflection from FE were used to determine stiffness values. Due to the irregularity of steel plate dimensions, particularly for the specimens BSTB and BSTI, all models have less stiffness than the reference model BSRH. As a result, fewer steel plates are located in the tension zone. The stiffness values are displayed in **Fig. 28** and **Table 8**.

Table 8. Summary of stiffness for all specimens

Model ID	Ultimate load P_u (kN)	Deflection at peck load Δ_u (mm)	Stiffness = P_u/Δ_y	Differenced in Stiffness %
BSRH (Ref.)	308.5	17.48	17.65	---
BSRM	298.8	18.71	15.97	- 9.52
BSRS	295.3	19.85	14.88	- 15.69
BSTB	245.4	20.63	11.89	- 32.63
BSTI	245.9	21.74	11.31	- 35.92
BSQC	315.6	18.41	17.14	- 2.89
BSQI	302.4	18.74	16.14	- 8.56

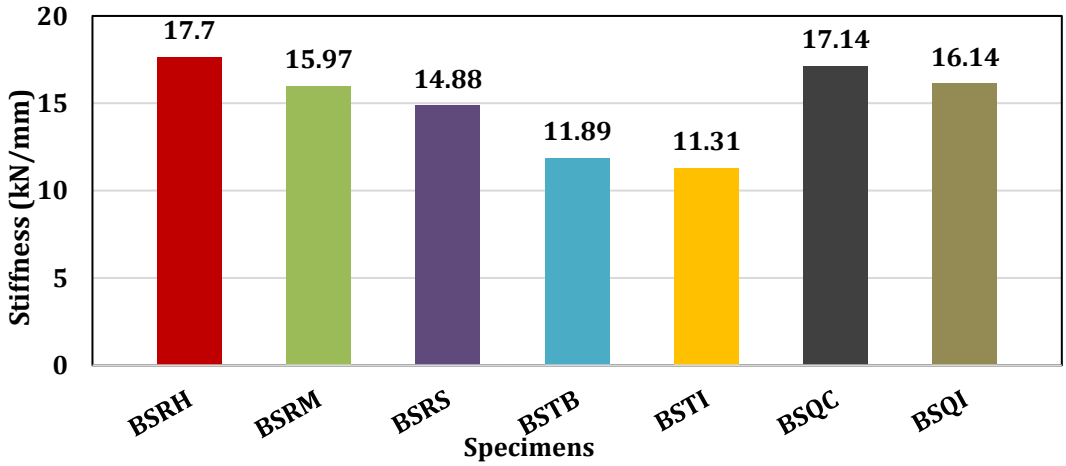

Figure 28. Stiffness for all specimens.

5.4 Ductility Index

The term "ductility index" refers to a member's capacity to tolerate inelastic deformations following yield deformation without experiencing a discernible decline in load capacity. Ductility is a crucial consideration when buildings for different stress situations. The load-deflection curves of flexural members can be used to determine their ductility index **(Hallawi et al., 2019; Hadeed et al., 2019)**. According to Eq. (6), the ductility index (μ) is the ratio of the failure deflection to the yield deflection.

$$\mu = \frac{\Delta_u}{\Delta_y} \tag{6}$$

Where, Δ_u is the deflection at peck load and, Δ_y is the deflection at yield section.
The ductility index results from yield and ultimate loading stage mid-span deflection values obtained from numerical analysis are shown in **Table 9** and **Fig. 29**. The results show that, in comparison to the reference model BSRH, the ductility index is higher in the models BSRM, BSRI, BSTB, BSTI, and BSQI by (1.69, 5.65, 184.74, 115.25, and 2.82 %), respectively. This increase was linked to the characteristics of the steel plates that rejoin the asymmetrical steel sections as a result of their combination stresses with the asymmetrical steel sections.

Table 9. Summary of ductility index for all specimens

Model ID	Deflection at yield Δ_y (mm)	Deflection at peck load Δ_u (mm)	Ductility index Δ_u/Δ_y	Difference in ductility index %
BSRH (Ref.)	9.9	17.48	1.77	---
BSRM	10.4	18.71	1.8	+ 1.69
BSRS	10.6	19.85	1.87	+ 5.65
BSTB	5.1	20.63	4.05	+ 184.74
BSTI	5.7	21.74	3.81	+ 115.25
BSQC	11.1	18.41	1.66	- 6.21
BSQI	10.3	18.74	1.82	+ 2.82

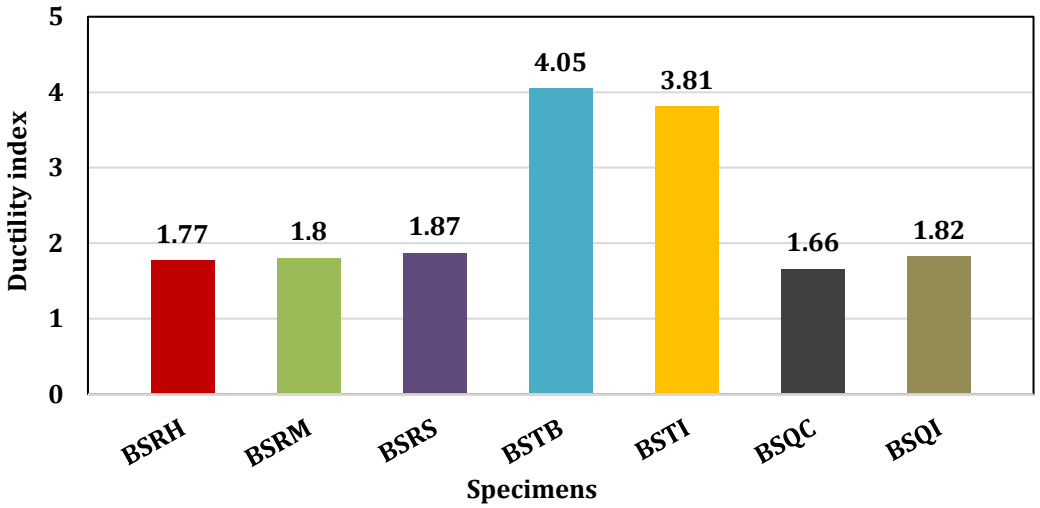

Figure 29. Ductility index for all specimens

6. CONCLUSIONS

Based on the results of the ABAQUS program, the following conclusions were drawn from the numerical analysis of composite concrete - asymmetrical IPE-section steel connected together by adding steel plates called (spacer) between two asymmetrical different halves subjected to two concentrated static loads, simply supported with:

- The ultimate load for specimens BSRM, BSRS, and BSQI slightly decreased by about 3.14%, 4.27%, and 1.98%, respectively, as compared to the reference model BSRH. However, due to the irregularity of the steel plate dimensions, the peak load effect dropped in specimens BSTB and BSTI by around 20.45% and 20.29%, respectively. When applied to curved steel plates to create non-concentration of stresses, the peak load for specimen BSQC increased by about 2.3% in comparison to reference specimens.
- The specimens BSRM, BSRS, BSTB, BSTI, BSQC, and BSQI showed an increase in beam deflection at the loading level of approximately 7.04%, 13.56%, 18.02%, 24.37%, 5.32%, and 7.21%, respectively, in comparison to the reference model.
- For the specimens BSRM, BSRS, BSTB, BDTI, and BSQI, the ductility index increased by approximately 1.69%, 5.65%, 184.74%, 115.25, and 2.82% in comparison to the reference model BSRH.
- This castellation steel member process has more structural efficiency and applicability since no waste is produced.
- The results were more realistic, with a uniform shape at the mid-height of the steel plate due to the reference specimen's rectangular plates.

- The FE analysis of parameterized nonlinearity is a highly reliable method of investigation. The challenges, time savings, cost, and labor associated with an experimental test make it the preferred method.

Overall, recommendations for future work include a numerical study of different shapes of steel plates to rejoin an asymmetrical steel section - composite concrete beams under strengthening by intermediate stiffeners and studying the effect of impact load or repeated load.

NOMENCLATURE

Symbol	Definition	Symbol	Definition
d_t	Scalar tension damage variable	μ	Ductility index
d_c	Scalar compression damage variable	$\varepsilon_c^{in,h}$	Inelastic compression strain of concrete
E_0	Initial Young's modulus	$\varepsilon_c^{pl,h}$	Plastic hardening strain in compression of concrete
f_r	Modulus of rupture, in MPa	ε_{cr}	Cracking strain
f_y	Yield Strength of Steel, in MPa	ε_{cu}	Strain of concrete corresponding in compression
P_u	Ultimate load to beam	ε_t	Nominal tension strain
t_w	Web thickness, in mm	ε_t^{ck}	Tension strain
t_f	Flange thickness, in mm	σ_c	Nominal compressive stress of concrete
Δ_u	Deflection at peak load, in mm	σ_t	Nominal tension stress
Δ_y	Deflection at yield, in mm	σ_{true}	True stress

Acknowledgements

The authors extend their appreciation to the Ministry of Higher Education for its assistance, as well as to the University of Baghdad. The authors thankful for the support received from Dean's Office of the College of Engineering and the head of the Civil Engineering Department throughout this endeavor.

Credit Authorship Contribution Statement

Wisam Hazim Khaleel: Writing the original draft, Software, Validation, and Methodology. Ahmed Jabbar Hussain Alshimmeri: Results analysis, proofreading and supervision.

Declaration of Competing Interest

The authors declare that they have no known competing financial interests or personal relationships that could have appeared to influence the work reported in this paper.

REFERENCES

ABAQUS, A., 2017. ABAQUS Analysis User's Manual Version 6.13. Assault Systems.

Abbas, N.Y., and Alshimmeri, A.J.H., 2024. Flexural behavior of a composite concrete castellated double channel steel beams strengthening with reactive powder concrete. *Tikrit Journal of Engineering Sciences*, 31(2), pp. 28-42. https://doi.org/10.25130/tjes.31.2.4

Abbas, N.Y., and Alshimmeri, A.J.H., 2024. Numerical study of composite concrete castellated double channel beams with strengthening techniques. *Journal of Engineering*, 30(02), pp. 30-51. https://doi.org/10.31026/j.eng.2024.02.03.

Abdul-Razzaq, K.S., Khaleel, W.H., and Dawood, A.A., 2023. Struts and ties realization in reinforced concrete ring deep beams. *ACI Structural Journal*, 120(4), pp. 151-164. https://doi: 10.14359/51738771.

Abidin, A.Z., and Izzuddin, B.A., 2013. Meshless local buckling analysis of steel beams with irregular web openings. *Engineering Structures*, *50*, pp. 197-206. https://doi.org/10.1016/j.engstruct.2012.10.006.

ACI Committee 318, 2019. Building code requirements for structural concrete (ACI 318M-19) and commentary (318R-19). American Concrete Institute, Farmington Hills, Michigan. USA.

Ahmed, A., and Said, A.M.I., 2024. The Effect of opening size and expansion ratio on the flexural behavior of hot rolled wide flange steel beams with expanded web. *Engineering, Technology & Applied Science Research*, 14(1), pp. 13033-13040. https://doi.org/10.48084/etasr.7254.

Al-Hilali, A.M., and Izzet, A.F., 2023. 3D-ABAQUS modelling of prestressed concrete hunched beams with multi-openings of different shapes. *Journal of Engineering*, 29(08), pp. 149-170. https://doi.org/10.31026/j.eng.2023.08.11.

Alkloub A, Allouzi R., and Naghawi H., 2019. Numerical non-linear buckling analysis of tapered slender reinforced concrete columns. *International Journal of Civil Engineering*. 17(8), pp. 1227-40. https://doi.org/10.1007/s40999-019-00395-5.

Al-Tameemi, S.K., and Alshimmeri, A.J., 2023, February. Behavior of asymmetrical castellated composite girders by gap in steel web. *In AIP Conference Proceedings* (Vol. 2414, No. 1). AIP Publishing. https://doi.org/10.1063/5.0116809.

Al-Zuhairi, A.H., Mansi, A.I., and Anbar-Iraq, B., 2017, May. Behavior of composite concrete castellated steel beams in flexure. *In 1st International Conference on Recent Trends of Engineering Sciences Sustainability* (Vol. 5).

American Institute of Steel Construction Inc. (AISC), Steel Construction Manual (15th Edition), 2016.

ASTM A36/A36M, 2014. Standard Specification for Carbon Structural Steel. United States

Basher, M.A., Shanmugam, N.E., and Khalim, A.R., 2009. Web openings in horizontally curved composite plate girders. *Journal of Constructional Steel Research*, 65(8-9), pp. 1694-1704. https://doi.org/10.1016/j.jcsr.2009.02.009.

Dawood, A.A., Abdul-Razzaq, K.S., and Abdulsahib, W.S., 2024. Experimental and finite element analysis of deep curved box girders: impact of concrete strength and geometry. *Diyala Journal of Engineering Sciences*, pp. 114-135. https://doi.org/10.24237/djes.2024.17407.

Dawood, A.A., Abdul-Razzaq, K.S., and Abdulsahib, W.S., 2024. Theoretical and experimental comparison between straight and curved continuous box girders. *Open Engineering*, 14(1), P. 20240085. https://doi.org/10.1515/eng-2024-0085.

Demir, A., Ozturk, H., and Dok, G., 2016. 3D Numerical modeling of RC deep beam behavior by non linear finite element analysis. *Disaster Science and Engineering*, 2(1), pp. 13-18.

Dionisio, M.C., 2004. Determination of critical location for service load bending stresses in non-composite cellular beams (Doctoral dissertation, Villanova University).

En, B., 2005. 1-1; Eurocode3: Design of Steel Structures: Part 1-1: General Rules and Rules for Buildings. European Committee for Standardization.

Fang, C., Wang, W., Qiu, C., Hu, S., MacRae, G.A., and Eatherton, M.R., 2022. Seismic resilient steel structures: A review of research, practice, challenges and opportunities. *Journal of Constructional Steel Research*, 191, P. 107172. https://doi.org/10.1016/j.jcsr.2022.107172.

Hadeed, S.M., and Alshimmeri, A.J.H., 2019. Comparative study of structural behaviour for rolled and castellated steel beams with different strengthening techniques. *Civil Engineering Journal*, 5(6), pp. 1384-1394. http://dx.doi.org/10.28991/cej-2019-03091339.

Hafezolghorani, M., Hejazi, F., Vaghei, R., Jaafar, M.S.B., and Karimzade, K., 2017. Simplified damage plasticity model for concrete. *Structural engineering international*, 27(1), pp. 68-78. https://doi.org/10.2749/101686616X1081.

Hagen, N.C., Larsen, P.K., and Aalberg, A., 2009. Shear capacity of steel plate girders with large web openings, Part I: Modeling and simulations. *Journal of constructional steel research*, 65(1), pp. 142-150. https://doi.org/10.1016/j.jcsr.2008.03.014.

Hallawi, A.F., and Al-Ahmed, A.H.A., 2019. Enhancing the behavior of one-way reinforced concrete slabs by using laced reinforcement. *Civil Engineering Journal*, 5(3), pp. 718-728. http://dx.doi.org/10.28991/cej-2019-03091282.

Hognestad, E., 1951. A study of Combined Bending and Axial Load in R.C. Members. M.Sc. Thesis, Civil Engineering Department, University of Illinois Engineering Exp. Sta. Bull. No.399.

Kerdal, D. and Nethercot, D.A., 1984. Failure modes for castellated beams. *Journal of Constructional Steel Research*, 4(4), pp. 295-315. https://doi.org/10.1016/0143-974X(84)90004-X.

Li, W., Wang, J., Xing, X., Liu, H., Di, J., Sun, X., Li, L., Li, H., and Qin, F., 2024. Investigation of shear behavior in high-strength bolt connectors for steel–concrete composite beams. *Materials*, 17(24), P. 6168. https://doi.org/10.3390/ma17246168.

Lubliner, J., Oliver, J., Oller, S., and Onate, E., 1989. A plastic-damage model for concrete. *International Journal of Solids and Structures*, 25(3), pp. 299-326. https://doi.org/10.1016/0020-7683(89)90050-4.

Naji, A., and Kadhim, M.F., 2025. Structural performance of double castellated steel beams with innovative opening configuration. *Engineering, Technology & Applied Science Research*, 15(2), pp. 20616-20622. https://doi.org/10.48084/etasr.9734

Ollgaard, J.G., Slutter, R.G., and Fisher, J.W., 1971. Shear strength of stud connectors in lightweight and normal-weight concrete. *Engineering Journal*, 8(2), pp. 55-64. https://doi.org/10.62913/engj.v8i2.160.

Oukaili, N.K., and Abdullah, S.S., 2017. Behavior of composite concrete-castellated steel beams under combined flexure and torsion. *In APFIS2017-6th Asia-Pacific Conference on FRP in Structures* (pp. 19-21).

Radic, I., Markulak, D., and Varevac, D., 2008. Numerical simulation of lateral stability of castellated beams. *In EUROSTEEL 2008, 5th European Conference on Steel and Composite Structures* (pp. 1593-1598).

Redwood, R., and Demirdjian, S., 1998. Castellated beam web buckling in shear. *Journal of Structural Engineering*, 124(10), pp. 1202-1207. https://doi.org/10.1061/(ASCE)0733-9445(1998)124:10(1202).

Tsavdaridis, K.D. and D'Mello, C., 2012. Optimisation of novel elliptically-based web opening shapes of perforated steel beams. *Journal of Constructional Steel Research*, 76, pp. 39-53.https://doi.org/10.1016/j.jcsr.2012.03.026.

الدراسة العددية لتكوينات مختلفة من صفائح الفولاذية لإعادة ربط مقطع فولاذي غير متماثل – عتبات خرسانية مركبة

وسام حازم خليل*، احمد جبار حسين الشمري

قسم الهندسة المدنية، كلية الهندسة، جامعة بغداد، بغداد، العراق

الخلاصة

هذه دراسة التحقق عددياً (النظري) على تأثير اشكال مختلفة من صفائح الحديدية الملحومة على سلوك مقاطع حديدية غير متماثلة ذات العصب الموسع المفتوح–عتبات خرسانية مركبة. تؤدي زيادة عمق العصب للعتبات الحديدية غير المتناظرة في الخرسانة المركبة الى زيادة الصلابة والقوة. زيادة عمق العصب يؤدي الى تحسين قوة وأداء العتبات الحديدية الخرسانية المركبة في سيناريوهات تصميم محددة، مثل، العتبات الخرسانية المركبة ذات المقاطع الحديدية اما موسعة، او قلعوية، او ذات شكل دائريي. يؤدي القطع الافقي في العصب في كل قسم من المقاطع الغير متناظرة الى انشاء عصب موسع من المقاطع الحديدية الغير متماثلة. بعد ذلك تجميع قطعتين من حرف (T) باللغة الإنجليزية غير المتماثلتين، وأضافه صفيحة تعرف باسم صفيحة الفاصلة التي تكون ذات مساحة ثابتة واشكال مختلفة تقع بين نصفين (T) باللغة الإنجليزية غير المتماثلتين. تم استعمال تحليل العناصر المحددة (FEA) الذي تم تطويره بواسطة برنامج (ABAQUS) الذي وضف لتطوير وتقييم نماذج عددية جديدة نماذج عددية جديدة من خلال اشكال مختلفة من صفائح الفاصلة التي انتجت المزيد من النماذج في وقت وتكلفة اقل. تشير النتائج الى ان الصفائح المنحنية زادت من سعة التحميل القصوى. بينما أدت الاشكال الأخرى الى انخفاض الصلادة. وبالتالي، زادت سعة التحميل القصوى للصفائح المنحية بمقدار 2.3% مقارنة مع النموذج المرجعي نتيجة لتقليل توزيع الاجهادات.

الكلمات المفتاحية: العتبات الخرسانية المركبة، اللدونة التالفة للخرسانة، توسيع العصب، موديل العناصر المحدودة، انبعاج العصب